Finite-Volume Time-Domain Simulations of MRI RF Coils by Subcell Circuit-Driven Thin-Wire Models

Ian Jeffrey and Joe LoVetri

Department of Electrical and Computer Engineering
University of Manitoba, Winnipeg, MB, R3T 5V6, Canada
ijeffrey@ee.umanitoba.ca, Joe_LoVetri@umanitoba.ca

Abstract: The modeling flexibility of an FVTD thin-wire subcell model that permits arbitrary wire orientation within the computational domain is shown to be well-suited to the simulation of tunable MRI RF coils where the tuning capacitors are modeled by subcell circuits. The circuits provide boundary conditions to the thin-wire model and do not impose any limitations on the volumetric mesh. Numerical results are provided to demonstrate the capabilities of the algorithm.

Keywords: Finite-Volume Time-Domain, Thin-Wire Models, Circuit Models, MRI

1. Introduction

In recent years, the finite-volume time-domain (FVTD) algorithm for solving Maxwell's equations has been applied to a variety of field problems [1-3]. FVTD for electromagnetic simulations is a robust algorithm and has been supplemented with a limited set of subcell models including the thin-wire model developed in [1]. Unfortunately, the model in [1] requires the thin-wires to conform to the edges of prismatic elements placing constraints on mesh generation. Recently, Holland-Simpson based thin-wire models [4] have been modified to permit arbitrary orientation within the computational domain for both the finite-difference (FD) and finite-element (FE) time-domain methods [5,6]. This model has been adapted to FVTD and supplemented with subcell-circuit boundary conditions [7]. In this paper, we demonstrate the flexibility of the thin-wire and circuit models to provide accurate simulations of the RF loop transceivers used in MRI environments.

2. The FVTD Algorithm

Herein, we consider a cell-centered, upwind, flux-split implementation of the FVTD algorithm [1,3]. The computational domain V is partitioned into N_V first-order polyhedral finite-volumes (or cells) V_i, each having an associated volume $|V_i|$. Each polyhedral volume is bounded by a set of K_i flat facets symbolized by $\partial V_{i,k}$. The medium associated with the i^{th} volume is simple and constant such that the permittivity is ϵ_i [F/m], the permeability is μ_i [H/m], and the conductivity is σ_i [S/m]. The continuous FVTD equations on each V_i are obtained from Maxwell's two curl equations integrated over each V_i:

$$\frac{d}{dt}\vec{\boldsymbol{U}}_i(t) = -\frac{1}{|V_i|}\sum_{k=1}^{K_i}\int_{S_{i,k}} \bar{\bar{\boldsymbol{\alpha}}}_i^{-1}\cdot\bar{\bar{\boldsymbol{A}}}_{i,k}\cdot\vec{\boldsymbol{U}}(t,\vec{r})dS + \bar{\bar{\boldsymbol{\alpha}}}_i^{-1}\cdot(\bar{\bar{\boldsymbol{\sigma}}}_i\cdot\vec{\boldsymbol{U}}_i(t)+\vec{\boldsymbol{S}}_i(t)). \tag{1}$$

The solution $\vec{\boldsymbol{\mathcal{U}}}(t,\vec{r}) \in \mathbb{R}^6$ at position $\vec{r}$ and time t contains both the electric field $\vec{\mathcal{E}}(t,\vec{r})$ [V/m] and the magnetic field $\vec{\mathcal{H}}(t,\vec{r})$ [A/m] *i.e.* $\vec{\boldsymbol{\mathcal{U}}}(t,\vec{r}) = [\vec{\mathcal{E}}(t,\vec{r})^T\ \vec{\mathcal{H}}(t,\vec{r})^T]^T$ where T denotes transposition. The source vector $\vec{\boldsymbol{\mathcal{S}}}(t,\vec{r}) = [-\vec{\mathcal{J}}(t,\vec{r})^T\ \vec{0}^T]^T$ supports impressed current densities $\vec{\mathcal{J}}(t,\vec{r})$ [A/m^2] under a total field formulation. The medium is represented by the two diagonal matrices $\bar{\bar{\boldsymbol{\alpha}}}_i = \text{diag}(\epsilon_i, \epsilon_i, \epsilon_i, \mu_i, \mu_i, \mu_i)$, $\bar{\bar{\boldsymbol{\sigma}}}_i = \text{diag}(-\sigma_i, -\sigma_i, -\sigma_i, 0, 0, 0)$. The quantities $\vec{\boldsymbol{\mathcal{U}}}_i(t)$ and $\vec{\boldsymbol{\mathcal{S}}}_i(t)$, respectively denote the volumetric averages of the solution and source vectors over V_i. A time-marching update to Maxwell's equations is obtained by associating an approximation to the average solution $\vec{\boldsymbol{\mathcal{U}}}_i(t)$ to each V_i, and time-integrating (1) where the surface values $\vec{\boldsymbol{\mathcal{U}}}(t,\vec{r})$, $\vec{r} \in \partial V_i$ are to be reconstructed from the cell-average solutions. Details are available in [1-3].

3. The Thin-Wire Model

Thin-wires are modeled within the FVTD algorithm as a subcell-model based on the method of Holland and Simpson [4], modified such that the wires can be arbitrarily oriented within the computational domain by using a distributional interpolation scheme [5,6]. For notational simplicity we consider a single wire existing in the domain $W \subset V$ that is discretized into segments (one dimensional finite-volumes) W_j, $j = 1, \ldots, N_W$. Assuming straight wire-segments, each one-dimensional finite-volume is directed in the $\hat{\zeta}_j$ direction, has barycentre ζ_j and is bounded by two points (facets) located at $\zeta_{j,k} = \zeta_j + k \cdot |W_j|/2$, where $|W_j|$ is the length of the segment. The thin-wire update equations are obtained from static approximations in the vicinity of the wire and by enforcing conservation of charge in W [4-7]. Integrating the resulting equations over each W_j and applying the divergence theorem leads to a set of (one-dimensional) FVTD equations. With $\boldsymbol{\mathcal{U}}_j(t) \in \mathbb{R}^2$ we have:

$$\frac{d}{dt}\boldsymbol{\mathcal{U}}_j(t) = -\frac{1}{|W_j|}\sum_{k=-1}^{1} k \cdot \bar{\bar{a}}_j \cdot \boldsymbol{\mathcal{U}}(t,\zeta_{j,k}) - \bar{\bar{b}}_i \cdot \boldsymbol{\mathcal{U}}_j(t) + \bar{\bar{c}}_j \cdot \boldsymbol{\mathcal{S}}_j(t). \tag{2}$$

The solution vector $\boldsymbol{\mathcal{U}}(t,\zeta) = [\mathcal{V}(t,\zeta)\ \mathcal{I}(t,\zeta)]^T$ where $\mathcal{V}(t,\zeta)$ [V] and $\mathcal{I}(t,\zeta)$ [A], respectively, define the voltage and current along the wire coordinate. Analogous to the three-dimensional case $\boldsymbol{\mathcal{U}}_j(t)$ denotes a segment-average of the solution and is associated, by approximation, with each segment. The source vector is given by $\boldsymbol{\mathcal{S}}(t,\zeta) = [0\ \langle\mathcal{E}_\zeta(t,\zeta)\rangle]^T$ where $\langle\mathcal{E}_\zeta(t,\zeta)\rangle$ is a weighted sum of the longitudinal electric field. The 2×2 matrices $\bar{\bar{a}}_j$, $\bar{\bar{b}}_j$ and $\bar{\bar{c}}_j$ are:

$$\bar{\bar{a}}_j = \begin{bmatrix} 0 & \frac{1}{C_j} \\ \frac{1}{L_j} & 0 \end{bmatrix} \quad \bar{\bar{b}}_j = \begin{bmatrix} \frac{G_j}{C_j} & 0 \\ 0 & \frac{R_j}{L_j} \end{bmatrix} \quad \bar{\bar{c}}_j = \begin{bmatrix} \frac{1}{C_j} & 0 \\ 0 & \frac{1}{L_j} \end{bmatrix}, \tag{3}$$

where the segment-dependent parameters per-unit-length parameters L_j, C_j, R_j, and G_j are constructed using the physics of the wire segment and the homogeneous medium surrounding the segment.

4. Wire-to-Field Coupling

From the formulation in the previous section, it is apparent that the fields couple to the thin-wire model by the term $\langle\mathcal{E}_\zeta(t,\zeta)\rangle$. Coupling from the wire to the field occurs through a current density $\vec{\mathcal{J}}(t,\vec{r})$ supported by $I(t,\zeta)$ on the wire. This current contributes to the source term $\vec{\boldsymbol{\mathcal{S}}}(t,\vec{r})$ in (1). The current density supported by the wire domain W is given by [5,6]:

$$\vec{\boldsymbol{\mathcal{J}}}(t,\vec{r}) = \sum_{j=1}^{N_W} I(t,\zeta) g(\rho) \Phi_j(\zeta) \hat{\zeta}, \tag{4}$$

where $g(\rho)$ is the same weighting function used to produce $\langle \mathcal{E}_\zeta(t,\zeta)\rangle$ (ρ being a radial distance from the wire to the point $\vec{r}$) and where $\Phi_j = 1$ iff $\zeta \in W_j$. The function $g(\rho)$ has finite support in the ρ direction, limiting the thin-wire influence to a distance $\rho_0 = 1.7\Delta$ where Δ is the average edge length of the volumetric discretization in the mesh. Details can be found in [5] and [6].

5. Thin-Wire Boundary Conditions by Subcell Circuits

The solution to the one-dimensional thin-wire equations is formulated in terms of an upwind, flux-split FVTD algorithm that ensures numerical stability of the discrete scheme. Upwinding of the spatial operator in (2) reformulates the operator $\bar{\bar{a}}_j(k) = k\bar{\bar{a}}_j$ into a positive part $\bar{\bar{a}}_j^+(k)$ and a negative part $\bar{\bar{a}}_j^-(k)$ by means of an eigen decomposition [7]. The system (2) becomes:

$$\frac{d}{dt}\boldsymbol{\mathcal{U}}_j(t) = -\frac{1}{u(W_j)}\sum_{k=-1}^{1}\left(\bar{\bar{a}}_j(k)^+\cdot\boldsymbol{\mathcal{U}}^+(t,\zeta_{j,k}) + \bar{\bar{a}}_j^-(k)\cdot\boldsymbol{\mathcal{U}}^-(t,\zeta_{j,k})\right) - \bar{\bar{b}}_i\cdot\boldsymbol{\mathcal{U}}_j(t) + \bar{\bar{c}}_j\cdot\boldsymbol{\mathcal{S}}_j(t) \quad (5)$$

where the boundary state $\boldsymbol{\mathcal{U}}^+(t,\zeta_{j,k})$ is the reconstructed solution at $\zeta_{j,k}$ from inside W_j while $\boldsymbol{\mathcal{U}}^-(t,\zeta_{j,k})$ is reconstructed from outside W_j. Due to this flux-splitting, the FVTD thin-wire formulation permits using subcell circuits to enforce the state $\boldsymbol{\mathcal{U}}^-(t,\zeta_{j,k})$ when W_j is terminated at facet k by a circuit. Motivated by the multiport-network, transmission-line formulation of LoVetri and Lapohos [8], we couple the circuit model to the thin-wire model using characteristic theory and formulate the circuit system using modified nodal analysis (MNA). The result is a volumetric-mesh-independent model that supports multiport subcell circuit networks connected to multiple thin-wires. We consider circuits consisting of $P+1$ nodes and corresponding nodal voltages v_p, $p = 0,\ldots,P$ referenced to $v_0 = 0$ $[V]$. MNA seeks to determine the nodal voltages by enforcing Kirchoff's current law (KCL) at each node by introducing an *auxiliary current* and a corresponding *auxiliary equation* on circuit branches where the current cannot be explicitly written in terms of the nodal voltages. Assuming that M auxiliary equations are required to solve a circuit with P nodes (excluding the reference node), we can obtain the following matrix equation:

$$\bar{\bar{G}}\cdot\vec{U}(t) + \bar{\bar{C}}\cdot\frac{d}{dt}\vec{U}(t) = \vec{S}(t) \quad (6)$$

where the matrices $\bar{\bar{G}}$ and $\bar{\bar{C}}$ have dimension $(P+M)$, the $(P+M)$-length solution vector $\vec{U}$ consists of the P unknown nodal voltages followed by the M auxiliary currents and where the $(P+M)$-length source vector $\vec{S}$ accounts for forcing functions and initial conditions. The first P rows of the system of equations corresponds to KCL at each of the P non-reference nodes. The remaining M equations impose the auxiliary equations.

Subcell circuits are introduced into the volumetric mesh at wire-segment terminals as shown, for example, by the double-box in Figure 1. This example circuit exists at terminal $\zeta_{j,1} = \zeta_{\ell,-1}$ and connecting segments W_j and W_ℓ. The MNA system accounts for the wires as follows:

- For each thin-wire segment connected to node p in the circuit we introduce an auxiliary current leaving node p. For the simple voltage source in Figure 1 this introduces the auxiliary currents i_1 and i_2. The auxiliary current i_s accounts for the current through the voltage source.
- We assume that the thin-wire voltage is the difference of two nodal voltages in the circuit. This assumption is required to ensure that the circuit and thin-wire models are referenced in a unified fashion. For the example circuit, the segments are differentially driven and we can assume that the wires are referenced to 0 [V] at node 0.

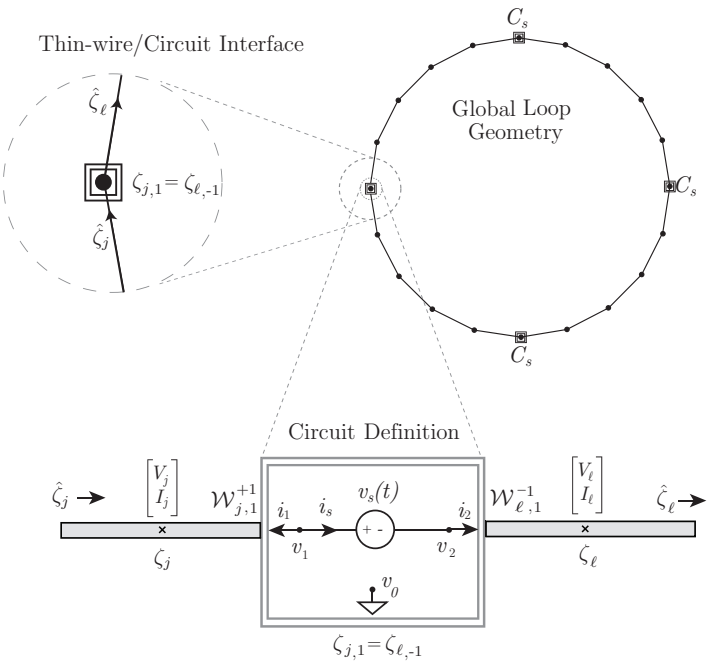

Fig. 1. A subcell circuit-driven thin-wire domain.

- Corresponding to the thin-wire auxiliary currents, we introduce auxiliary equations based on the characteristics of the thin-wire equations. It can be shown that the characteristics

$$\mathcal{W}_j^{\pm}(t,\zeta) = (V(t,\zeta) \pm Z_j I(t,\zeta))/2, \quad \zeta \in W_j \tag{7}$$

propagate unchanged along segment j in the $\pm\zeta$ direction. Here, $Z_j = \sqrt{L_j/C_j}$ is the segment impedance. The assumption of coupled thin-wire/circuit voltage referencing allows us to write the characteristics flowing into the circuit in terms of the nodal voltages and auxiliary currents. For the example circuit, the W_j junction provides the equation $\mathcal{W}_j^{+}(t,\zeta_{j,1}) = (v_1 - Z_j i_1)/2$ while the W_ℓ junction gives $\mathcal{W}_\ell^{-}(t,\zeta_{\ell,-1}) = (v_2 + Z_\ell i_2)/2$. The characteristics are regarded as inputs to the circuit system and are to be reconstructed from the segment-average values.

For the example circuit in Figure 1, the MNA system can be written as:

$$\begin{bmatrix} 0 & 0 & 1 & 0 & 1 \\ 0 & 0 & 0 & 1 & -1 \\ 1 & 0 & -Z_j & 0 & 0 \\ 0 & 1 & 0 & -Z_\ell & 0 \\ 1 & -1 & 0 & 0 & 0 \end{bmatrix} \cdot \begin{bmatrix} v_1 \\ v_2 \\ i_1 \\ i_2 \\ i_s \end{bmatrix} = \begin{bmatrix} 0 \\ 0 \\ 2\mathcal{W}_{j,1}^{+1}(t) \\ 2\mathcal{W}_{\ell,-1}^{-1}(t) \\ v_s(t) \end{bmatrix} \tag{8}$$

where $\bar{\bar{C}}$ is zero. The first two equations enforce KCL at nodes 1 and 2. The third and fourth (auxiliary) equations enforce the constitutive relationship between the circuit quantities and the thin-wire characteristics. The last equation is an auxiliary relationship between the voltage source and the nodal voltages. The solution to the matrix equation is used to compute the segment flux $\bar{\bar{a}}_j^{-}(k) \cdot \boldsymbol{\mathcal{U}}^{-}(t,\zeta_{j,k})$ whenever segment j is connected to a circuit on facet k. In the case of the example circuit, this results in $\boldsymbol{\mathcal{U}}^{-}(t,\zeta_{j,1}) = \begin{bmatrix} v_1 & -i_1 \end{bmatrix}^T$, $\boldsymbol{\mathcal{U}}^{-}(t,\zeta_{\ell,-1}) = \begin{bmatrix} v_2 & i_2 \end{bmatrix}^T$. This method is

completely general. An arbitrary number of thin-wire segments can be connected to an arbitrary circuit. The construction of the matrix equation, incoming characteristics and segment fluxes is easily automated with minimal book-keeping. In addition, the time-history of the circuit solution can be stored to provide a simple mechanism for computing system parameters.

6. Numerical Results

The subcell-driven thin-wire model detailed in the previous sections provides a flexible formulation for the three-dimensional field simulation of complex thin-wire geometries driven by arbitrary sub-cell circuits. This flexibility makes the model especially attractive to the numerical simulation of MRI RF coils. As a test case, we consider a metallic loop 18.2 [cm] in diameter. The diameter of the conductor (modeled as PEC) is taken to be 2 [mm]. The circumference of the wire is then $0.182\pi \approx 0.5718$ [m] and is a half-wavelength at $\lambda = 1.1435$ [m] or at 262.3 [MHz].

The wire is embedded in an 80 [cm] diameter spherical volumetric domain, truncated by Silver-Müller boundary conditions [1], and is excited by the circuit shown in Figure 1 with $v_s(t)$ given by the derivative of a gaussian pulse having mean $t_\mu = 2\times10^{-9}$ and deviation $t_\sigma = 6\times10^{-10}$ resulting in appreciable energy in the 200 to 700 [MHz] range. Two discretizations of the computational domain are considered. Mesh one (M1) permits a maximum frequency of around 700 [MHz] resulting in roughly 80-thousand three-dimensional volumes and exactly 48 thin-wire segments. Mesh two (M2) permits a maximum frequency of around 1300 [Mhz] resulting in roughly 450-thousand three-dimensional volumes and exactly 100 thin-wire segments. It was found in [5,6] that the simulation of thin-wire loops requires enforcing conditions on $\vec{\mathcal{J}}(t,\vec{r})$ in equation (4) to conform to the curvature of the wire. We adopt the same approach presented in detail in [6].

The FVTD simulation of the problems was performed using a fourth-order Runge-Kutta time-integration scheme. Convergence required $15,000$ time-steps for M1 and $16,000$ time-steps for $M2$. The input impedance $Z_{in}(f)$ to the loop antenna was extracted by storing $v_s(t)$ and $i_s(t)$ at each step and computing the frequency-domain result:

$$Z_{in}(f) = \frac{\mathcal{F}\{v_s(t)\}(f)}{\mathcal{F}\{-i_s(t)\}(f)}, \tag{9}$$

where $\mathcal{F}\{\}$ denotes the Fourier transform. The real part of the input impedance for the simple loop is shown for both the M1 and M2 discretizations in Figure 2(a). An analytic value for the inductance of the loop gives $L = 0.525\times10^{-6}$ [H].

We now show how this loop can be tuned for MRI applications at $f_{\text{MRI}} = 64$ [MHz] by adding a series or parallel capacitance C to the loop given by:

$$2\pi f_{\text{MRI}} = \frac{1}{\sqrt{LC}} \rightarrow C = \frac{1}{(2\pi 64\times10^6)^2 L} = 11.78[\text{pF}]. \tag{10}$$

This capacitance is introduced in series with the loop by adding three series capacitors $C_s = 3C$ as subcell circuits at the three locations denoted by C_s in Figure 1. To ensure that sufficient energy is present in the 64 [MHz] range we modify $v_s(t)$ such that $t_\mu = 1\times10^{-8}$ and $t_\sigma = 3\times10^{-9}$. The input admittance computed by the FVTD engine for the loop/capacitor system is shown in Figure 2(b) demonstrating resonance near 64 [MHz]. The peaks are at 65.6 [MHz] (M1) and 65 [MHz] (M2) and are within 3 percent of f_{MRI}.

7. Conclusions

The FVTD subcell thin-wire model coupled with arbitrary lumped-circuit elements provides an elegant way to perform full-field simulations of MRI RF circuity. Future work will consider more complicated MRI structures such as body coils with RF cabling.

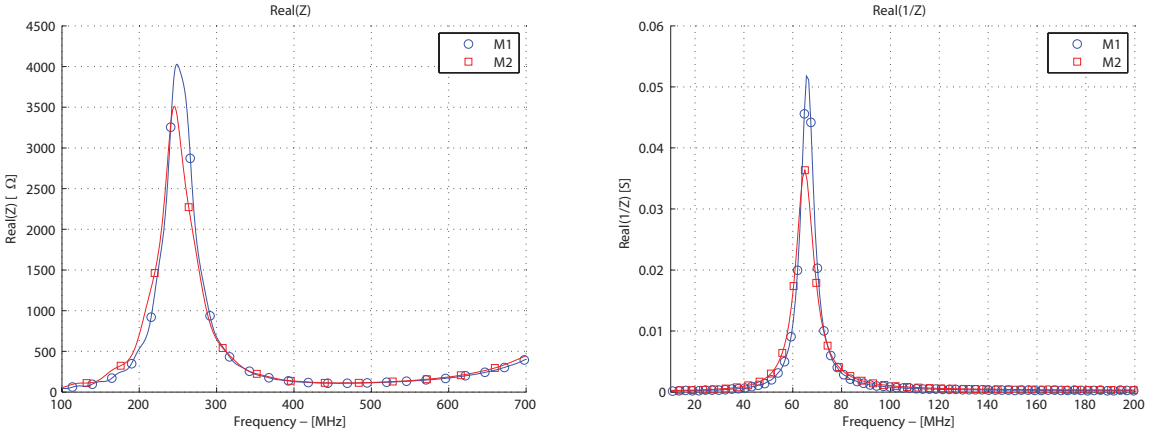

(a) (b)

Fig. 2. (a) Input resistance of the simple loop. (b) Input conductance of the tuned loop.

8. References

[1] P. Bonnet, X. Ferrières, B. Michielsen, and P. Lotz, "Finite-volume time-domain method," in *Time Domain Electromagnetics*, S. M. Rao, Ed. New York: Academic, 1997, pp. 307-367, ch. 9.

[2] C. Fumeaux, D. Baumann, and R. Vahldieck "Finite-Volume Time-Domain analysis of a cavity backed archimedean spiral antenna," *IEEE Transactions on Antennas and Propagation*, vol. 54, pp. 844-851, 2006.

[3] D. Firsov, J. LoVetri, I. Jeffrey, V. Okhmatovski, C. Gilmore and W. Chamma, "High-order FVTD on unstructured grids using an object-oriented finite-volume time-domain computational engine," *ACES Journal*, vol. 22, no .1, pp. 71-82, March 2007.

[4] R. Holland and L. Simpson, "Finite-difference analysis of EMP coupling to thin struts and wires," *IEEE Transactions on Electromagnetic Compatibility*, vol. EMC-23, no. 2, pp. 88-97, May 1981.

[5] F. Edelvik, "A new technique for accurate and stable modeling of arbitrarily oriented thin wires in the FDTD method," *IEEE Transactions on Electromagnetic Compatibility*, vol. 45, no. 2, pp. 416-423, May 2003.

[6] F. Edelvik, G. Ledfelt, P. Lötstedt, and D. J. Riley, "An unconditionally stable subcell model for arbitrarily oriented thin wires in the FETD method," *IEEE Transactions on Antennas and Propagation*, vol. 51, no. 8, pp. 1797-1805, August 2003.

[7] I. Jeffrey and J. LoVetri, "FVTD Thin-Wire Models Terminated by Arbitrary Lumped-Element Circuits," ACES 2010, Tampere Finland, 25-29 April 2010.

[8] J. LoVetri and T. Lapohos, "Explicit upwind schemes for lossy MTL's with linear terminations," *IEEE Transactions on Electromagnetic Compatibility*, vol. 39, no. 3, pp. 189-200, August 1997.